Applied Physics A (2022) 128:529
https://doi.org/10.1007/s00339-022-05674-y

Applied Physics A
Materials Science & Processing

The materialization of an impedimetric biosensor to detect papillomavirus DNA based on indium oxide nanowires

S. H. Reza Shojaei[1,2] · Sourena Ramezani Emame[3] · Mohammad Mahdi Afrouz[3] · Mohsen Shariati[1,3]

Received: 25 February 2022 / Accepted: 9 May 2022 / Published online: 26 May 2022

Abstract

In this study, the impedimetric biosensor of human papillomavirus DNA (HPV DNA) in label-free approach based on indium oxide nanowires (In_2O_3 NWs) was fabricated. The fabrication of In_2O_3 NWs was successfully conducted using the thermal evaporation method and catalyst-free approach. The grown NWs had a diameter of about 70–90 nm and a length of several microns. The fabricated electrode was able to show high selectivity by changing the relative charge transfer resistance of 80, 60 and 50% for complementary, mismatch and non-complementary sequences, respectively. The electrode biosensor was stable for up to 6 weeks under the effect of electric field and showed 93% of its initial response sensitivity and detected DNA hybridization at very low concentrations in a linear response range from 0.1 pM to 0.1 μM. The In_2O_3 NWs showed a detection of limit (LOD) 20 fM. The behavior of negatively charged DNA oligonucleotides in a nanostructured array under the influence of electric field brought about NWs in the preferred direction with an excellent analytical response. Compared to current biosensors, the designed and fabricated biosensor, in a suitable sensing mechanism, was able to optimize response sensitivity and stability and also could improve the reproducibility conditions.

Keywords Biosensor · Papillomavirus · In_2O_3 nanowires · Impedance spectroscopy · Label-free mechanism

1 Introduction

Human papilloma virus infection is a type of human papilloma virus (HPV), [1]. Most of the human papilloma virus infections are symptom free and not resolved automatically [1–4]. In some patients, the human papillomavirus infection causes warts or pre-cancerous ulcers, [1]. There are three classified categories, comprising about 200 types of papilloma viruses. Depending on their role in the development of cervical cancer, they are denominated as low-risk, moderate and high-risk categories [2–8]. The high-risk genetic species of the HPV has a significant role in the engenderment of cervical cancer, and this is the third most common cancer in the post-endometrial women and ovarian cancer in the United States [2]. Cancer resulting from HPV infection is one of the leading causes of mortality worldwide and the second leading cause of morbidity among women in developing countries [2, and 8]. Among the 14 known high-risk species of the human papillomaviruses, two of them, subspecies HPV16 and HPV18, are the most important high-risk genotypes around the world and they have been monitored in 62% of the cases related to cervical cancer. About 93% of the cervix-related cancers can be prevented; thus, their diagnosis and recognition are extremely vital [2]. Due to its low sensitivity and specificity, the detection of the HPV via cell culture and serological testing may not be easy [2–4]. In contrast, molecular cervical cancer screening techniques including hybrid capture assay tests and polymerase chain reaction (PCR) are efficient techniques for the detection of HPV [4]. However, the mentioned techniques are basically dependent on the DNA sensing of viruses, and the preparation and purification of samples in these techniques are very challenging and excessively time consuming [6–8].

Functional materials have been a strong candidate to overcome the problems due to the lack of energy and systematic deficiencies [9–11]. The continuous evolution of

✉ Mohsen Shariati
Shariatimohsen59@gmail.com

[1] Department of Physics, Faculty of Science, Sahand University of Technology, P.O. Box, Tabriz 5331817634, Iran

[2] X-LAB, Hasselt University, Agoralaan D, 3590 Diepenbeek, Belgium

[3] Manzaryeh Danesh School, Danesh Complex Institute, Tehran, Iran

nanoscience and nanotechnology in recent years has led to the production of quasi-one-dimensional structures in a variety of different morphologies such as NWs, core shell NWs, nanoribbons, nanotubes, hierarchical heterogeneous micro and nanostructures, porous hollow nano-boxes, nanosheets, layered paraelectric/ferroelectric nanocomposite polymers [12–25], nanorods and nanopores [26–28]. Among the various nanostructured materials which have been produced, metal oxides have received special attention [29, 30]. Metal oxide nanostructures have received a great deal of attention due to their fundamental properties and wide application in the manufacture of electronic components [31–34]. Among them, In_2O_3, with an optical gap of about 3.6 eV, has important applications in areas such as window heaters, solar cells, and gas sensors [26]. Recently, In_2O_3 nanostructures have received considerable attention due to their properties and applications in the field of bio-sensing [27], gas sensing [28, 35–38] and nano-transistors [39]. There has recently been a great deal of interest in the synthesis and research of In_2O_3 nanostructures. Some of the different In_2O_3 nanostructures, which have been obtained by different methods, such as CVD method [36 and 37], pulsed-laser [40], and oxide powder evaporation method [41], were applied to small analytes such as streptavidin [42].

Indium oxide has recently been used in biosensing and analyte measurements [37]. In some reports, indium-based materials were used for HPV detection. Cervical cancer caused by HPV infection was investigated by a label-free nano-sensing platform [43]. A fast, accurate and early detection platform was developed for HPV-16 detection in cost-effective label-free DNA based on an electrochemical biosensor. A low-cost and rapid electrochemical resistive DNA biosensor based on the current relaxation method was described [44]. A DNA probe, complementary to the specific human papillomavirus type 16 (HPV-16) sequence, was immobilized onto a screen-printed gold electrode. DNA hybridization was detected by applying a potential step of 30 mV to the system, composed of an external capacitor and the modified electrode DNA/gold, for 750 µs and then relaxed back to the OCP, at which point the voltage and current discharging curves were registered for 25 ms.

Electrochemical impedance spectroscopy (EIS) detection is one of the most promising mechanisms in label-free biosensing, especially in DNA detection. The EIS measurement studies the dielectric parameters of a biological system in wide frequencies [45–48]. The EIS provides information on basic processes such as surface adsorption, charge transfer, ion exchange and diffusion [45–49]. The EIS provides the fundamental and functional information at the interface between the electrode and electrolyte [45–47]. Electrochemical impedance measurement, as a non-destructive and relatively easy to use detection system, has been widely used in the field of label-free biosensors that are sensitive to cell culture monitoring, interaction between antibody and antigen [45–51], and DNA oligonucleotides hybridization [46–49].

In this study, the impedimetric biosensor of HPV DNA based on In_2O_3 NWs was fabricated. In this paper, the fabrication of In_2O_3 NWs using thermal evaporation method in catalyst-free method in a horizontal tube furnace was successfully conducted. The fabricated electrode was able to give high selectivity by changing the relative charge transfer resistance for complementary, mismatch and non-complementary sequences. The electrode biosensor was stable for several weeks under the effect of electric field and detected DNA hybridization at very low concentrations. The behavior of negatively charged DNA oligonucleotides in a nanostructured array under the influence of electric field brought about NWs in the preferred direction with an excellent analytical response. Compared to current biosensors, the designed and fabricated biosensor, in a suitable sensing mechanism, was able to optimize response sensitivity and stability and also could improve the reproducibility conditions.

2 Experimental

2.1 Materials

Potassium chloride, $K_4Fe(CN)_6$, $K_3Fe(CN)_6$, ethanol, HCl, NaCl, EDTA (ethylenediaminetetraacetic acid), and $Na_3C_6H_5O_7$ were purchased from Merck. The PC template was obtained from Whatman Co. The phosphate-buffered saline (PBS), dithiothreitol (DTT), $NiSO_4{\cdot}6H_2O$, H_3BO_3, $KAu(CN)_2$, CH_2Cl_2, 3-aminopropyltriethoxysilane (APES), and PVP (polyvinylpyrrolidone) were prepared from Sigma-Aldrich.

2.2 Analyte preparation

The surface modification for HPV DNA probe's immobilization on the Au-decorated nanowires (gold coated for FESEM imaging) was performed in a sterilized clean room. Immobilization of thiolated oligonucleotides probe was initially performed after DNA preparation by DTT. PBS (6 µL) (pH ~ 4.5) containing 100 µM single-stranded DNA probe was transported on the electrode (modified nanowires) for 12 h. After DNA drop on the electrode surface, for removing some of the unabsorbed DNA oligonucleotides, the electrode system was submerged into 4 mM 6-mercapto-1-hexanol for 1 h and then cleansed by PBS and DDW. For hybridization of the SS-DNA probe with the DNA target, first, the probe electrode was submerged in PBS solution in pH ~ 7.5, at a concentration of 15 µM SS-DNA target for 6 h. It is important to note that the target was part of the DNA sequence of the HPV and

it was a complementary strand to the DNA probe. Finally, the sensing part of the setup was cleansed with DDW and dried with argon gas at a suitable flow. The buffers used in this work were as follows: DNA immobilization buffer: buffer Tris–EDTA (TE, 10 mM Tris–HCl, 1 mM EDTA, pH 8.0); hybridization buffer: 2 × saline sodium citrate (SSC, 300 mM NaCl, 20 mM $Na_3C_6H_5O_7$, pH 7.0). The electrolyte solution was 0.2 M KCl containing 2 mM $K_4Fe(CN)_6/K_3Fe(CN)_6$ (1:1). All solutions were prepared in deionized water (DI water). 25-mer ss-DNA sequence with HS-$(CH_2)_6$-modification at the 5′-end with HPLC purification (as HPV 16 probe) and all target oligonucleotides with BIO-RP purification were provided. Stock solutions (100 µM) of the DNA sequences were prepared with sterile distilled water (SD water) and stored in a refrigerator at − 20 °C. Specificity of the oligonucleotide sequences was investigated with Basic Local Alignment Search Tool (BLAST) [5]. The oligonucleotides sequences used are listed in Table 1.

2.3 NWs fabrication

In this experiment, the source used was indium oxide powder. In this work, there was no catalyst. A number of P-type silicon substrates, immersed in ethanol alcohol solution for 20 min, were distilled twice in water solution for about 20 min. 0.025 g of the powder was placed in an alumina boat in the hot zone of a tube. The working process of the coating was followed: first, the inside chamber was vacuumed by a rotary pump up to the allowable limit, to a pressure of 10^{-3} mbar. When the pressure reached this level, the furnace temperature was raised to about 900 °C. Then argon gas was allowed to enter the chamber as a carrier gas in the alumina tube at a flow rate of 25 sccm. The duration of the deposition was about 2 h. Finally, a white layer settled on the substrates. The structural and crystalline properties of the samples were analyzed using an XRD analyzer system (Siemens Model 500D; λ = 0.15419 nm, CuKα) and the surface properties were analyzed by an FESEM analyzer (200FEG, Hitachi). A schematic illustration of this deposition process is shown in Fig. 1.

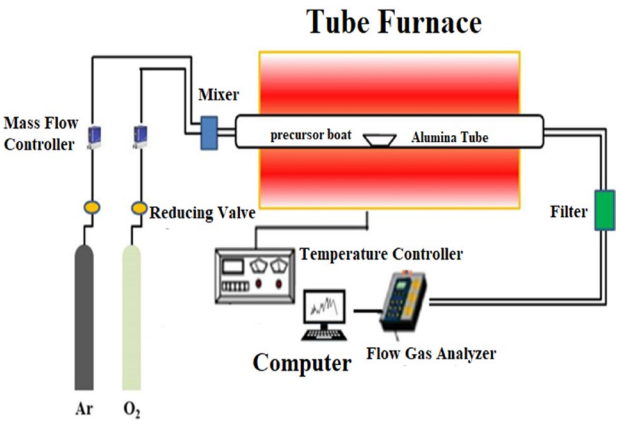

Fig. 1 Thermal evaporation furnace; indium oxide deposition in the presence of argon gas

2.4 Electrochemical impedance spectroscopy measurements

Electrochemical impedance spectroscopy (EIS) measurements were conducted by a PG STAT302N automatic potentiostat equipped with a frequency response analyzer module (FRA32) (Autolab, Metrom, The Netherlands), associated with an electrochemical cell in a three-electrode system which Ag/AgCl as reference, Pt as counter, and In_2O_3 as a working electrode. To plot Nyquist diagrams, Tecplot 360 software was used along with the computational fluid dynamic formats (CFD). EIS measurements were performed in the frequency range of 0.01–100 kHz and the disturbance potential was + 10 mV. Measurements were performed under OCP conditions related to bias voltage. All EIS measurements were performed three times.

3 Results and discussion

3.1 Structural and surface analysis

Figure 2 shows the FESEM image of the fabricated samples. In this image, as can be seen, there are NWs with a diameter of 70–90 nm and a length of several microns. In such methods, the growth mechanism is usually called VS. In some methods associated with a catalyst, the catalytic

Table 1 The HPV16 DNA oligonucleotides sequences

Sequence name	Sequence of oligonucleotides	Company (Country)
Thiolated-probe	5′-SH-AAAGCAAAGTCATATACCTCACGTC-3′	Bioneer Corporation (South Korea)
Complementary	5′-GACGTGAGGTATATGACTTTGCTTT-3′	Bioneer Corporation (South Korea)
One-point Mismatch	5′ - ACG CCA GAT GAA GAA GGG GAC GGT A - 3′	Bioneer Corporation (South Korea)
Non-complementary	5′-AACGTGAGGTATATGACTTTGCTTT-3′	Bioneer Corporation (South Korea)

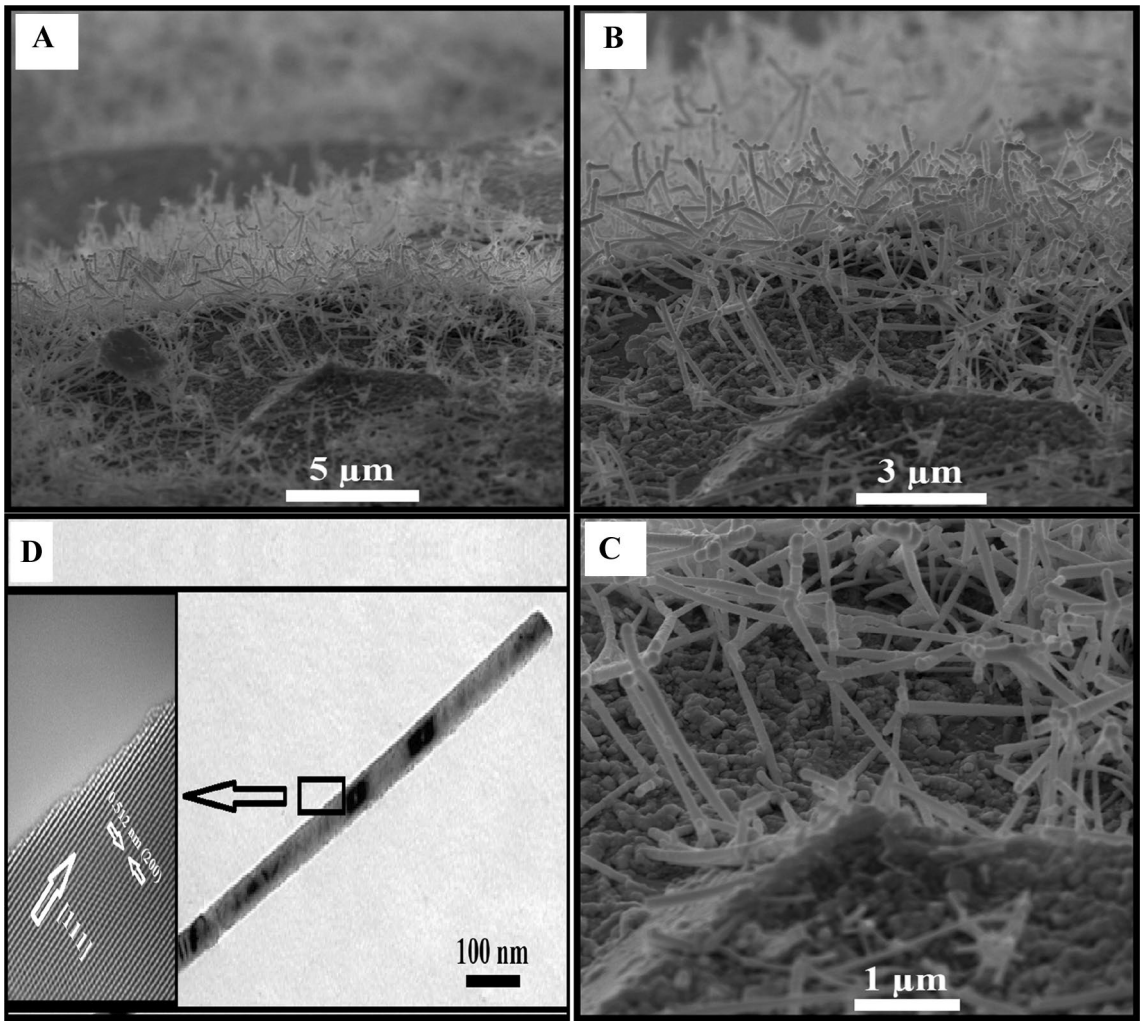

Fig. 2 The FESEM image of indium oxide NWs. The scale for **A** 5 µm, **B** 3 µm and **C** 1 µm, **D** the HRTEM and TEM image of In_2O_3 NW

nanoparticles are clearly visible at the end of the needle nanostructure; however, these are absent in the NWs. The NWs were grown in an uncontrollable direction due to the lack of catalysts. The needle-like structures began to grow strongly from any point that caused the growth of NWs in an intertwined and intangible design. In this method, nucleation sites were created, due to the use of the VS mechanism, by indium oxide vapor particles. This method does not require an external catalyst. The indium oxide atoms themselves provide these nucleation sites in a very interesting way and form these structures. The HRTEM and TEM measurements of an In_2O_3 NW are shown in Fig. 2D. In Fig. 2D the growth direction is coincided with the In_2O_3 NWs. The crystallographic plane of In_2O_3 for cubic crystal lattice by the interplanar spacing of 0.512 nm related to the (200) crystallographic plane was validated in Fig. 2D. The growth direction of fabricated NWs were oriented to [111], [28, 36, 37].

Figure 3 shows the XRD analysis of the fabricated NWs. Interestingly, the formation of highly crystalline

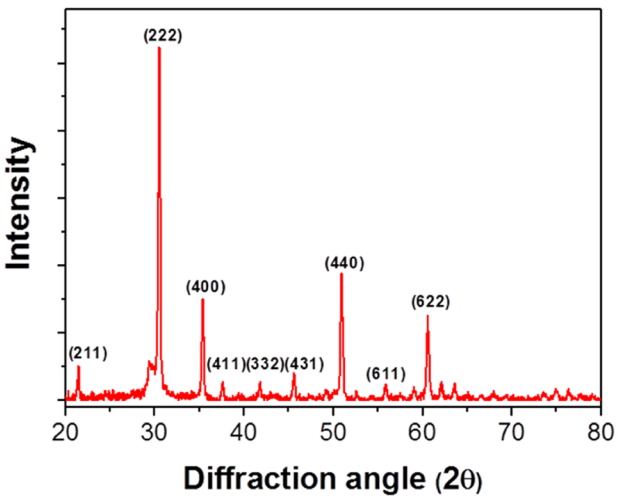

Fig. 3 Spectrum of indium oxide NWs by XRD analysis

nanostructures occurs in one direction. The formation of indium oxide structures is mainly significant in this regard. The absence of a catalyst can be attributed to the creation of related structures in an uncontrollable direction. The nanostructures created in this experiment are crystallized along a length that is completely arbitrary and random. According to the reference [36, 37, 52], the cellular constant of these nanostructures is $a = 1.012°$ nm according to JCPDS No. 6-0416.

3.2 Growth mechanism

There are two models to describe the growth mechanism of one-dimensional materials. The model associated with this section is a common torsional growth mechanism that emphasizes the existence of a rotational dislocation, which extends parallel to the axis of the wire or rod [26]. In this model, the plate rotates perpendicular to the dislocation line, causing the growth step to act as a low-energy site [26]. When the growth of NWs is achieved through direct condensation of the vapor phase without the use of a catalyst, the growth method used is called vapor–solid (VS) [26]. This method is sometimes called self-catalysis. In the past, this growth process was thought to be due to network defects, but when the NW was observed to be defective, this explanation was no longer acceptable. Another surprising effect recorded in this method is that the NW growth rate is higher than the computational density of the vapor phase. This can be interpreted as the plates in the NW structure absorbing the molecules were later dispersed on the main growth surfaces of the wire. The VS process occurs in many non-catalytic growth processes. According to the information obtained from a series of relatively complete theoretical and experimental works, it has been shown that the minimization of surface free energy causes the growth of VS [26]. At high temperatures, the precursor material evaporates and then condenses directly on the substrate in the low temperature range. When the condensation process takes place, the molecules are first condensed from catalytic granules, which act as nucleation sites [26]. As a result, they enable direct growth to minimize the surface energy that dominates the growth process. In other words, when indium oxide vapor particles are generated in the said conditions in a very hot region, they are transported by the carrier gas, i.e., argon, and land on the silicon substrate at a lower temperature [26]. These particles themselves cause the process of nucleation, adsorption and growth of NWs using the torsional growth process. In this type of growth, the NWs which are bent and twisted, absorb molecules or clusters of vapor which ultimately leads to one-dimensional growth of indium oxide NWs.

3.3 Sensory analysis

The sensing measurements were conducted in several tests such as selectivity, response, stability, reproducibility, calculating the calibration curves and Randels equivalent circuit parameters. Figure 4 shows the schematic image of DNA

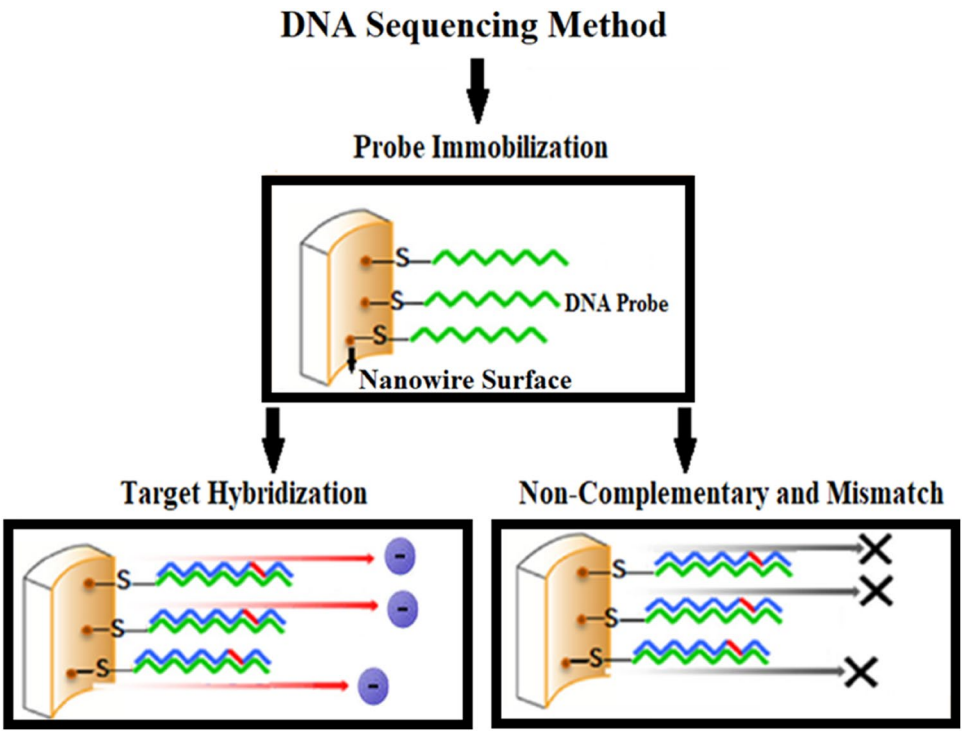

Fig. 4 The schematic image of DNA immobilization and hybridization on the NW surface

immobilization and hybridization on the NW surface. As shown in Fig. 4, the immobilization process occurs on the NW surface. For target hybridization, which is coupling the single strand (probe) with the complementary strand, the signal response results in a larger number of charge carriers in the electrolyte. Uniform and continuous deposition of oligonucleotides on the NW surface is a main parameter for DNA sensing. For non-complementary and mismatch sequences, the weak signal is sensed. In weak hybridization, the response recording process is conducted in low concentration of the charge carriers.

3.3.1 Selectivity measurement for In_2O_3 electrode

Figure 5 shows the EIS spectrum (Nyquist curve Z' vs. Z'') using redox ions for the oligonucleotide-modified electrode. The Randles parameters, R_{ct}, CPE and R_S, show the charge transfer resistance, the constant phase element at the interface between the electrode and the electrolyte, and the electrolyte resistance due to the uncompensated resistance to the solution associated with the internal resistance of the electrode and the resistance of the connections and wires, respectively. The Z_W (Warburg impedance) resistance to the release of ferro/ferri ions in the electrode/electrolyte interfaces originates from the redox couple diffusion and the electrode at low frequencies [53]. Results are obtained after three different independent tests for probe, complementary, mismatch and non-complementary DNA targets. All experiments were measured at a concentration of 1 µM. Figure 5 indicates the selectivity of the surface of an In_2O_3 electrode

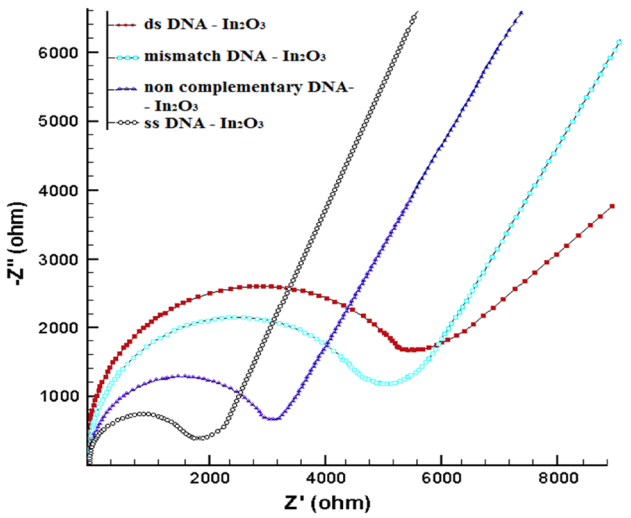

Fig. 5 The EIS impedance spectra for probes, complementary target, mismatch and non-complementary DNA oligonucleotides at 1 µM. The electrolyte solution: 0.2 M KCl solution containing 2 mM $K_4Fe(CN)_6/K_3Fe(CN)_6$ (1:1). Impedance spectra using AC modulation from + 10 mV in the frequency range of 0.01 Hz to 100 kHz with DC bias without changes due to open circuit potential

with ss-DNA, complementary, non-complementary, and mismatch oligonucleotides. In Fig. 5, the EIS impedance spectra for the electrode modified with the ss-DNA probe and their hybridization for biosensors were investigated. As shown in Fig. 5, due to the compatibility and correlation of In_2O_3 NWs with DNA targets, the diameter of the impedance semicircles of the In_2O_3 electrode increased sharply in the presence of complementary oligonucleotides that show the reduction of the electrical conductivity of the In_2O_3 electrode system. Figure 5 shows that the In_2O_3 modified electrode has significant DNA-sensing capabilities. The corresponding charge transfer resistance (R_{ct}) for dsDNA–In_2O_3 and ssDNA–In_2O_3 electrodes are 5618 and 1806 ohms, respectively. The diameter of the single-stranded DNA hybridization circle stabilized on the In_2O_3 substrate with the complementary target strand increased compared to the non-complementary hybridization. The diameter of the probe hybridization semicircle compared to non-complementary hybridization increased with the target hybridization. This means that the charge transfer resistance enhanced with the formation of the complementary double layer and the change is around the value of $\Delta R_{ct} = 3812\ \Omega$. Due to the electrostatic repulsion interactions, EIS measurements using non-complementary oligonucleotides indicate faster charge transfer kinetics and reduced resistance than with the complementary single strand. However, in comparison to the immobilized complementary DNA strand, Nyquist plots show an enhancement in resistance when the non-complementary and single strand with a different base were used. Compared to probes, the electrostatic repulsion between the ferro/ferri redox couples and In_2O_3 increases the charge transfer resistance. Also, the slope of the Warburg linear region for the complementary strand due to changes in the amount of penetration resistance of the charged species was reduced. By forming the double-stranded DNA, enhancement of the penetration resistance of charged species into the interface layer increased the Warburg's impedance, causeing the mass transfer regime changes.

3.3.2 EIS response for In_2O_3 electrode

The sensitivity of the In_2O_3 electrode response was examined in the presence of virus DNA. This study was performed by testing the response of the fabricated biosensor to different concentrations of complementary target oligonucleotides. The sensitivity of the biosensor response to complementary sequences for In_2O_3 was measured from 0.1 pM to 0.1 µM (Fig. 6). No satisfactory response was recorded for concentrations less than 1 µM. The In_2O_3 electrode was able to respond to 0.1 pM. The amount of charge transfer resistance increased with increasing target DNA concentration of the complementary sequences. The strands of DNA molecules form a self-assembling single

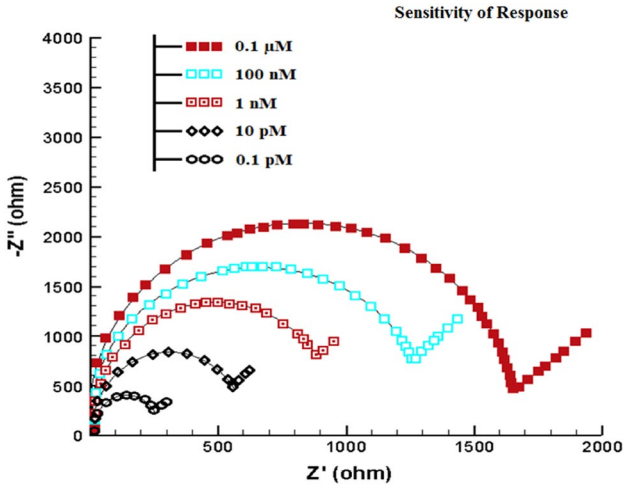

Fig. 6 EIS response measurements for the In_2O_3 electrode. Biosensor sensitivity to complementary sequences measured for In_2O_3 from 0.1 pM to 0.1 µM electrolyte solution 0.2 M KCl including 2 mM $K_4Fe(CN)_6/K_3Fe(CN)_6$ (1: 1). Impedance spectra using AC modulation from + 10 mV in the frequency range of 0.01 Hz to 100 kHz with DC bias and without changes due to open circuit potential

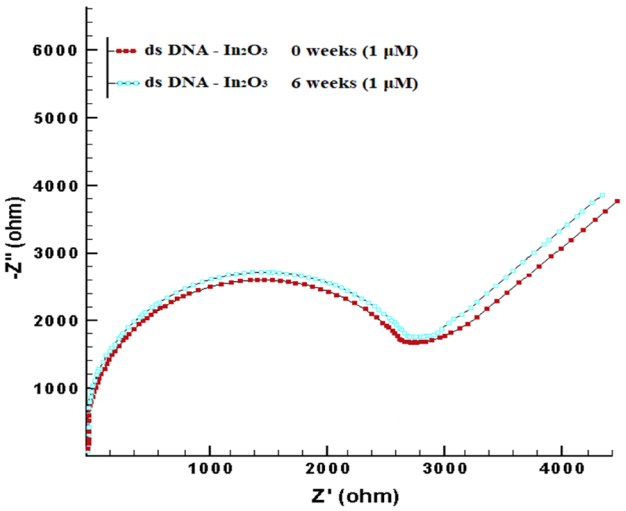

Fig. 7 Stability of In_2O_3 electrode by storage in freezer at 4 °C for 6 weeks (blue curve). Results of response to the complementary target (at a concentration of 1 µM). Recovery of 93% of the initial sensor response. Electrolyte solution; 0.2 M KCl solution containing 2 mM $K_4Fe(CN)_6/K_3Fe(CN)_6$ (1: 1). Impedance spectra using AC modulation from + 10 mV in the frequency range of 0.01 Hz to 100 kHz with DC bias and without changes due to open circuit potential

layer on the electrode surface due to the strong covalent bond of thiol to gold [54]. Changes in charge transfer resistance occurred due to conformational changes that occurred during DNA hybridization [54]. As the concentration of electroactive ions increases, the charge transfer resistance decreases. On the other hand, the enhancement of the concentration of complementary DNA led to an increase in charge transfer resistance due to the formation of compressed and aggregative layer. In fact, electrostatic interaction and spatial inhibition between ferro–-ferri species and DNA phosphate group prevent ions from reaching the electrode surface and create a higher potential barrier for electron transfer of these species [54]. Also, the diffusion control zone has the lowest slope in the case of complementary filaments with higher concentration, which in turn is related to the more complete composition formed in the presence of complementary filaments at higher concentrations, which has the lowest possibility of mass transfer. However, it provides a self-aggregating monolayer on the surface of thiol-plated gold electrode [54].

3.3.3 The stability test for fabricated In_2O_3 electrode

The stability of the In_2O_3 electrode was investigated by storing biosensors in the freezer at 4 °C; after 6 weeks the results showed a maximum response for In_2O_3 (at a concentration of 1 µM), and the In_2O_3 biosensor was able to obtain 93% of its initial responses (Fig. 7). This showed that the In_2O_3 biosensor response has long-term stability.

3.3.4 Calibration curves for In_2O_3 electrode

Figure 8 shows the calibration curve for the In_2O_3 biosensor. Figure 8 shows that changes in charge transfer resistance indicate a linear relationship with the logarithm scale of the concentration of complementary DNA sequences in the range of 0.1 pM to 0.1 µM at the In_2O_3 electrode (Fig. 8, blue line). The information diagram clearly shows a high sensitivity of the In_2O_3 electrode response to the state without applying electrical potential. A detection limit of 20 fM

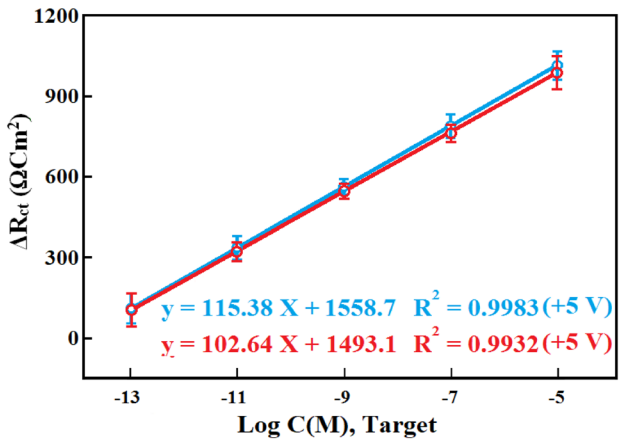

Fig. 8 Calibration curve for In_2O_3 biosensor (blue line). Calculation of sensor stability after 6 weeks of maintenance (red line)

was obtained for the In_2O_3 electrode [2]. It was estimated that $Y = S_b + 3\sigma_b$, where S_b is the signal of the blank and σ_b is the standard deviation of the blank. The ability of the biosensor was tested by storing the biosensor in the freezer at 4 °C for 6 weeks, Fig. 8 (red line). The results showed that the biosensor was able to maintain a maximum of 93% of its initial response after 6 weeks. This indicates that the impedimetric biosensor responses were long-term stable.

3.3.5 Reproducibility for In_2O_3 electrode

The reproducibility of the In_2O_3 biosensor in DNA sensors was evaluated after calculating the data from three independent electrodes fixed at a concentration of 1 µM. Relative standard deviation (RSD) values for In_2O_3 were 0.62, 3.26 and 5.96% for non-complementary, mismatch and complementary targets, respectively. RSD values of less than 9% indicated that the In_2O_3 electrode had more acceptable biosensor detection than previous reports and had good accuracy for detecting and measuring HPV16 DNA [24, 55, 56].

3.3.6 Randles equivalent circuit parameters

The parameters of the Randles electric field elements obtained from the simulation of the impedance spectrum of the In_2O_3 electrode are shown in Table 2. EIS measurements were consistent with the circuit elements. The changes caused by the application of the field are quite noticeable. According to the conditions obtained, a higher sensitivity of the electrode can be achieved by fitting.

3.3.7 The comparison

To compare the quantification and qualification of the fabricated DNA biosensor, its performance described in several recently published works is summarized in Table 3. The results in Table 3 also show that the electrochemical response of the In_2O_3 electrode shows satisfactory performance and has better response. The experimental results reported in this study evidently demonstrate the effects of In_2O_3 electrode structure on the improvement of DNA sensor detection sensitivity.

4 Conclusion

A DNA biosensor was developed to detect human papillomavirus based on indium oxide NWs in asymptomatic mechanisms and electrochemical impedance measurements, as well as in accordance with the Randles equivalent circuit. The indium oxide NWs were successfully performed in a horizontal tube furnace using thermal evaporation method without the use of catalysts. The ss-DNA single-stranded DNA probe was covalently immobilized on the surface of the In_2O_3 NWs electrode by the thiol agent. The In_2O_3 electrode biosensor detected HPV DNA hybridization at very low concentrations in a linear response range from 0.1 pM

Table 2 Summary of Randels equivalent circuit parameters for In_2O_3 electrode

Sample	R_S (Ω)	CPE (10^{-6} µF)	N	R_{ct} (Ω)	RSD (%)	Z_W (10^{-5})
SS-DNA	34	326	0.82	1806	1.37	8.93
dS-DNA	108	183	0.89	5618	2.16	3.11

Table 3 Comparison of the quantification and qualification of the fabricated HPV DNA biosensors

Biosensor	Electrode	Method	Concentration range	LOD	Refs.
Biosensor based on labeled pyrrolidinyl peptide	Screen-printed carbon electrodes	SWV	0.02–12 µM	4 nM	[57]
DNA biosensor for HPV 16	Gold electrode	DPV	18–250 nM	18 nM	[58]
Biosensor for short DNA sequences	Screen-printed gold electrodes	SWV	0–770 pM	0.308 pM	[6]
Papillomavirus DNA biosensor using SWCNT	Single-walled carbon nanotube	EIS	1aM–1 µM	1 aM (Atto molar)	[4]
DNA biosensor to identify a target gene cloned into a plasmid	Pencil graphite electrode	DPV	5.36–670 nM	2 nM	[59]
A pencil graphite (lead) electrode (PGE) for the detection of HPV	Pencil graphite electrode	SWV	185–7700 nM	185 nM	[60]
An amperometric sensor for papillomavirus	Carbon nano-onion-modified glassy carbon	Amperometry	0–20 nM	0.5 nM	[61]
Impedimetric biosensor to detect papillomavirus	In_2O_3 NWs	EIS	0.1 pM to 0.1 µM	20 fM	This work

to 0.1 μM. In_2O_3 electrode biosensor was able to achieve a diagnostic limit of 20 fM. In_2O_3 electrode was able to make a strong differentiation between complementary, non-complementary and mismatch DNA sequences and was able to obtain high selectivity by changing the relative charge transfer resistance of 80, 60 and 50% for complementary, mismatch and non-complementary sequences, respectively. The In_2O_3 electrode biosensor was stable for up to 6 weeks and showed 93% of its initial detection response.

Funding There is no funding in this work.

Declarations

Conflict of interest The authors declare that they have no known competing financial interests or personal relationships that could have appeared to influence the work reported in this paper.

References

1. M. Van Ranst, J.B. Kaplan, R.D. Burk, Phylogenetic classification of human papillomaviruses: correlation with clinical manifestations. J. Gen. Virol. **73**(10), 2653–2660 (1992)
2. L.C. Brazaca, P.L.D. Santos, P.R. de Oliveira, D.P. Rocha, J.S. Stefano, C. Kalinke, R.A.A. Muñoz, J.A. Bonacin, B.C. Janegitz, E. Carrilho, Biosensing strategies for the electrochemical detection of viruses and viral diseases–a review. Anal. Chim. Acta **1159**, 338384 (2021)
3. M. Shariati, M. Ghorbani, P. Sasanpour, A. Karimizefreh, An ultrasensitive label free human papilloma virus DNA biosensor using gold nanotubes based on nanoporous polycarbonate in electrical alignment. Anal. Chim. Acta. **1048**, 31–41 (2019)
4. S. Wang, L. Li, H. Jin, T. Yang, W. Bao, S. Huang, J. Wang, Electrochemical detection of hepatitis B and papilloma virus DNAs using SWCNT array coated with Au nanotubes. Biosens. Bioelectron **41**, 205–210 (2013)
5. M. Shariati, Impedimetric biosensor for monitoring complementary DNA from Hepatitis B virus based on gold nanocrystals. J. Electrochem. Soc. **168**, 016512 (2021)
6. N. Zari, A. Amine, M.M. Ennaji, Label-free DNA biosensor for electrochemical detection of short DNA sequences related to human papilloma virus. Anal. Lett. **42**(3), 519–535 (2009)
7. N. Nasirizadeh, H.R. Zare, M.H. Pournaghi-Azar, M.S. Hejazi, Introduction of hematoxylin as an electroactive label for DNA biosensors and its employment in detection of target DNA sequence and single-base mismatch in human papilloma virus corresponding to oligonucleotide. Biosens. Bioelectron **26**(5), 2638–2644 (2011)
8. L.D. Tran, D.T. Nguyen, B.H. Nguyen, Q.P. Do, H. Le Nguyen, Development of interdigitated arrays coated with functional polyaniline/MWCNT for electrochemical biodetection: application for human papilloma virus. Talanta **85**(3), 1560–1565 (2011)
9. Q. Chu, Z. Sun, Y. Liu, H. Cui, B. Cheng, D. Dastan, K. Moon, G. Yang, C. Wong, Difluorobenzylamine treatment of organolead halide perovskite boosts the high efficiency and stability of photovoltaic cells. ACS Appl. Mater. Interfaces **14**(9), 11388–11397 (2022)
10. S. Xia, Z. Shi, L. Sun, S. Sun, D. Dastan, R. Fan, Suppressing the loss and enhancing the breakdown strengths of high-k materials via constructing layered structure. Mater. Lett. **312**, 131654 (2022)
11. M. Shariati, A. Mallakin, F. Malekmohammady, F. Khosravi-Nejad, Inhibitory effects of functionalized indium doped ZnO nanoparticles on algal growth for preservation of adobe mud and earthen-made artworks under humid conditions. Int. Biodeterior. Biodegradation **127**, 209–216 (2018)
12. L. Liang, Z. Shi, X. Tan, S. Sun, M. Chen, D. Dastan, B. Dong, L. Cao, Largely improved breakdown strength and discharge efficiency of layer-structured nanocomposites by filling with a small loading fraction of 2D zirconium phosphate nanosheets. Adv. Mater. Interfaces **9**(3), 2101646 (2021)
13. M. Kartha, B. Reshi, P. Walke, D. Dastan, Morphological study of thin films: simulation and experimental insights using horizontal visibility graph. Ceram. Int. **48**, 5066–5074 (2022)
14. L. Tao, J. Huang, D. Dastan, J. Li, X. Yin, Q. Wang, Flue gas separation at organic-inorganic interface under geological conditions. Surf. Interfaces **27**, 101462 (2021)
15. M. Shariati, F. Khosravinejad, The laser-assisted field effect transistor gas sensor based on morphological zinc-excited tin-doped In_2O_3 nanowires. Surf. Rev. Lett. **24**(08), 1750113 (2017)
16. M. Shariati, The continuous and persistent periodical growth induced by substrate accommodation in In_2O_3 nanostructure chains and their photoluminescence properties. Appl. Phys. A **118**(3), 997–1007 (2015)
17. M. Han, Z. Shi, W. Zhang, K. Zhang, H. Wang, D. Dastan, R. Fan, Significantly enhanced high permittivity and negative permittivity in Ag/Al_2O_3/3D-$BaTiO_3$/epoxy metacomposites with unique hierarchical heterogeneous microstructures. Compos. Part A **149**, 106559 (2021)
18. M. Shariati, M. Darjani, The lateral In_2O_3 nanowires and pyramid networks manipulation by controlled substrate surface energy in annealing evolution. J. Cryst. Growth **436**, 104–112 (2016)
19. M. Zhang, Z. Shi, J. Zhang, K. Zhang, L. Lei, D. Dastan, B. Dong, Greatly enhanced dielectric charge storage capabilities of layered polymer composites incorporated with low loading fractions of ultrathin amorphous iron phosphate nanosheets. J. Mater. Chem. C **9**, 10414 (2021)
20. M. Shariati, The Cancer therapy materialization by Theranostic nanoparticles based on gold doped Iron oxide under electromagnetic field amplification. Nanomed. Nanotechnol. Biol. Med. **35**, 102406 (2021)
21. L. Sun, Z. Shi, B. He, H. Wang, S. Liu, M. Huang, J. Shi, D. Dastan, H. Wang, Asymmetric trilayer all-polymer dielectric composites with simultaneous high efficiency and high energy density: a novel design targeting for advanced energy storage capacitors. Adv. Funct. Mater. **31**(35), 2100280 (2021)
22. S. Wei, Z. Shi, W. Wei, H. Wang, D. Dastan, M. Huang, J. Shi, S. Chen, Facile preparation of ultralight porous carbon hollow nanoboxes for electromagnetic wave absorption. Ceram. Int. **47**, 28014–28020 (2021)
23. S. Sun, Z. Shi, L. Sun, L. Liang, D. Dastan, B. He, H. Wang, M. Huang, R. Fan, Achieving concurrent high energy density and efficiency in all polymer layered paraelectric /ferroelectric composites via introducing a moderate layer. ACS Appl. Mater. Interfaces **13**, 27522–27532 (2021)
24. Y. Jiao, Z. Huang, W. Hu, X. Li, Q. Yu, Y. Wang, Y. Zhou, D. Dastan, In-situ hybrid Cr_3C_2 and γ'-Ni_3(Al, Cr) strengthened Ni matrix composites: microstructure and enhanced properties. Mater. Sci. Eng. A **820**, 141524 (2021)
25. N. Haghnegahdar, M. Abbasi Tarighat, D. Dastan, Curcumin-functionalized nanocomposite AgNPs/SDS/ MWCNTs for electrocatalytic simultaneous determination of dopamine, uric acid, and guanine in co-existence of ascorbic acid by glassy carbon electrode. J. Mater. Sci. Mater. Electron. **32**, 5602–5613 (2021)

26. J.G. Lu, P. Chang, Z. Fan, Quasi-one-dimensional metal oxide materials. Synthesis, properties and applications. Mater. Sci. Eng. R **52**, 49 (2006)
27. Q. Liu, Y. Liu, F. Wu, X. Cao, Z. Li, M. Alharbi, A.N. Abbas, M.R. Amer, C. Zhou, Highly sensitive and wearable In_2O_3 nanoribbon transistor biosensors with integrated on-chip gate for glucose monitoring in body fluids. ACS Nano **12**(2), 1170–1178 (2018)
28. M. Shariati, M. Sadeghi, Ultrasensitive DNA biosensor for hepatitis B virus detection based on tin-doped WO_3/In_2O_3 heterojunction nanowire photoelectrode under laser amplification. Anal. Bioanal. Chem. **412**, 5367–5377 (2020)
29. K. Shan, F. Zhai, Z. Yi, X. Yin, D. Dastan, F. Tajabadi, A. Jafari, S. Abbasi, Mixed conductivity and the conduction mechanism of the orthorhombic $CaZrO_3$ based materials. Surf. Interfaces **23**, 100905 (2021)
30. S. Nie, D. Dastan, J. Li, W. Zhou, S. Wu, Y. Zhou, X. Yin, Gas-sensing selectivity of n-ZnO/p- Co_3O_4 sensors for homogeneous reducing gas. J. Phys. Chem. Solids **150**, 109864 (2021)
31. L. Tao, J. Huang, D. Dastan, T. Wang, J. Li, X. Yin, Q. Wang, New insight into absorption characteristics of CO_2 on the surface of calcite, dolomite, and magnesite. Appl. Surf. Sci. **540**, 148320 (2021)
32. K. Shan, Z. Yi, X. Yin, D. Dastan, S. Dadkhah, B. Coates, H. Garmestani, Mixed conductivities of A-site deficient Y, Cr-doubly doped $SrTiO_3$ as novel dense diffusion barrier and temperature-independent limiting current oxygen sensors. Adv. Powder Technol. **31**, 4657–4664 (2020)
33. M. Asadzadeh, F. Tajabadi, D. Dastan, P. Sangpour, Z. Shi, N. Taghavinia, Facile deposition of porous fluorine doped tin oxide by Dr. Blade method for capacitive applications. Ceram. Int. **47**, 5487–5494 (2021)
34. L. Tao, J. Huang, D. Dastan, T. Wang, J. Li, X. Yin, Q. Wang, CO_2 capture and separation on charge−modulated calcite. Appl. Surf. Sci. **530**, 147265 (2020)
35. J.Y. Lao, J.Y. Huang, D.Z. Wang, Z.F. Ren, Self-assembled In_2O_3 nanocrystal chains and nanowire networks. Adv. Mater. **16**, 65 (2004)
36. M. Shariati, S. Alishavandi, Phototransistor properties of indium tin oxide nanowires grown by RF sputtering mechanism and annealing process. NANO **10**(01), 1550006 (2015)
37. M. Shariati, The ITO-Capped WO_3 nanowires biosensor based on field effect transistor in label-free protein sensing. Appl. Phys. A **123**(5), 370 (2017)
38. Z.L. Zhan, J.Q. Xu, D.G. Jiang, State of In_2O_3-based gas sensor. Chin. J. Trans. Technol **22**, 1 (2003)
39. J.T. Hu, T.W. Odom, C.M. Lieber, " Chemistry and physics in one-dimension: synthesis and properties of nanowires and nanotubes. Acc Chem. Res **32**, 435 (1999)
40. M.H. Huang, S. Mao, H. Feick, H. Yan, Y. Wu, H. Kind, E. Weber, R. Russo, P. Yang, Room-temperature ultraviolet nanowire nanolasers. Science **292**, 1897 (2001)
41. O. Hayden, A.B. Greytak, D.C. Bell, Core-shell nanowire light-emitting diodes. Adv. Mater **17**, 701 (2005)
42. X.Y. Kong, Z.L. Wang, Structures of indium oxide nanobelts. Solid State Commun. **128**, 1 (2003)
43. S. Pareek, U. Jain, M. Bharadwaj, N. Chauhan, A label free nanosensing platform for the detection of cervical cancer through analysis of ultratrace DNA hybridization. Sensing **33**, 100444 (2021)
44. J.R. Espinosa, M. Galván, A.S. Quiñones, J.L. Ayala, V. Ávila, S.M. Durón, Electrochemical resistive DNA biosensor for the detection of HPV type 16. Molecules **26**(11), 3436 (2021)
45. B. Kang, U. Yeo, K.H. Yoo, Anodized aluminum oxide-based capacitance sensors for the direct detection of DNA hybridization. Biosens. Bioelectron. **25**, 1592–1596 (2010)
46. Y.J. Kim, Y.J. Kim, J.E. Jones, H. Li, H. Yampara-Iquise, G. Zheng, C.A. Carson, M. Cooperstock, M. Sherman, Q. Yu, Three-dimensional (3-D) microfluidic-channel-based DNA biosensor for ultra-sensitive electrochemical detection. J. Electroanal. Chem. **702**, 72–78 (2013)
47. S. Wu, W.W. Ye, M. Yang, M. Taghipoor, R. Meissner, J. Brugger, P. Renaud, Impedance sensing of DNA immobilization and hybridization by microfabricated polycarbonate nanopore templates. Sens. Actuators B **216**, 105–112 (2015)
48. A. Santos, T. Kumeria, D. Losic, Nanoporous anodic aluminum oxide for chemical sensing and biosensors. Trends Anal. Chem. **44**, 25–38 (2013)
49. M.M. Rahman, X.B. Li, N.S. Lopa, S.J. Ahn, J.J. Lee, Electrochemical DNA hybridization sensors based on conducting polymers. Sensors **15**, 3801–3829 (2015)
50. W. Ye, Y. Xu, L. Zheng, Y. Zhang, M. Yang, P. Sun, A Nanoporous Polycarbonate template based electrochemical biosensor for histamine determination with biofunctionalized magnetic nanotubes concentration and signal amplification. Sensors **16**, 1767 (2016)
51. A. Bonanni, M.I. Pividori, M. del Valle, Impedimetric detection of influenza a (H1N1) DNA sequence using carbon nanotubes platform and Au nanotubes amplification. Analyst **135**(7), 1765–1772 (2010)
52. X.S. Peng, Y.W. Wang, X.F. Wang, L.X. Zhao, G.W. Meng, L.D. Zhang, Large-Scale synthesis of In_2O_3 nanowires. Appl. Phys. A **74**, 437 (2002)
53. Y. Tan, X. Wei, M. Zhao, B. Qiu, L. Guo, Z. Lin, H.H. Yang, Ultra-selective homogeneous electrochemical biosensor for DNA species related to oral cancer based on nicking endonuclease assisted target recycling amplification. Anal Chem **87**, 9204–9208 (2015)
54. Y.-T. Long, C.-Z. Li, T.C. Sutherland, H.-B. Kraatz, J.S. Lee, Electrochemical detection of single-nucleotide mismatches: application of M-DNA. Anal. Chem. **76**, 4059–4065 (2004)
55. P. Takmakov, I. Vlassiouk, S. Smirnov, Hydrothermally shrunk alumina nanopores and their application to DNA sensing. Analyst **131**, 1248–1253 (2006)
56. Z.G. Gokce, P. Akalın, F.N. Kok, A.S. Sarac, Impedimetric DNA biosensor based onpolyurethane/poly(m-anthranilic acid) nanofibers. Sens Actuators B **254**, 719–726 (2018)
57. S. Jampasa, W. Wonsawat, N. Rodthongkum, W. Siangproh, P. Yanatatsaneejit, T. Vilaivan, O. Chailapakul, Electrochemical detection of human papillomavirus DNA type 16 using a pyrrolidinyl peptide nucleic acid probe immobilized on screen-printed carbon electrodes. Biosens Bioelectron **54**, 428–434 (2014)
58. D.S. Campos-Ferreira, G.A. Nascimento, E.V.M. Souza, M.A. Souto-Maior, M.S. Arruda, D.M.L. Zanforlin, M.H.F. Ekert, D. Bruneska, J.L. LimaFilho, Electrochemical DNA biosensor for human papillomavirus 16 detection in real samples. Anal Chim Acta **804**, 258–263 (2013)
59. D.S. Campos-Ferreira, E.V.M. Souza, G.A. Nascimento, D.M.L. Zanforlin, M.S. Arruda, M.F.S. Beltrão, A.L. Melo, D. Bruneska, J.L. LimaFilho, Electrochemical DNA biosensor for the detection of human papillomavirus E6 gene inserted in recombinant plasmid. Arab J Chem **9**(3), 443–450 (2016)
60. R.E. Sabzi, B. Sehatnia, M.H. Pournaghi-Azar, M.S. Hejazi, Electrochemical detection of human papilloma virus (HPV) target DNA using MB on pencil graphite electrode. J Iran Chem Soc **5**(3), 476–483 (2008)
61. J.P. Bartolome, L. Echegoyen, A. Fragoso, Reactive carbon Nano-onion modified glassy carbon surfaces as DNA sensors for human papillomavirus oncogene detection with enhanced sensitivity. Anal Chem **87**(13), 6744–6751 (2015)